Z.J. Sun, P. Di Lizia, F. Bernelli Zazzera, Y.Z. Luo
High-Order State Transition Polynomial with Time Expansion Based on Differential Algebra
Acta Astronautica, In press-Published online 28/03/2019
doi:10.1016/j.actaastro.2019.03.068

High-Order State Transition Polynomial with Time Expansion based on Differential Algebra

Zhen-Jiang Sun*, Pierluigi Di Lizia†, Franco Bernelli-Zazzera‡, Ya-Zhong Luo§, Kun-Peng Lin¶

April 10, 2019

Abstract

In this study, a high-order state transition polynomial with time expansion (STP-T) method is developed to propagate an initial orbital state around its reference value to a variable final time based on the differential algebra (DA) technique. STP-T is a high-order Taylor polynomial of the final orbital state expanded around the reference initial state and reference propagation time. Since the final state usually shows different nonlinearity with respect to different components of initial state and propagation time, a weighted-order scheme is combined with STP-T, which enables the STP-T to have higher orders on the components with higher nonlinearity and lower orders on the components with lower nonlinearity. Then, an error estimation method is presented, which can a priori provide the error profiles of a STP-T and is useful for selecting a proper order and determining the corresponding valid ranges of displacements. Finally, the STP-T method is tested for orbit propagation under three typical orbital dynamics: the unperturbed Keplerian dynamics, the J_2 perturbed two-body dynamics, and the nonlinear relative dynamics. The numerical simulation results indicate that the STP-T supplies a good approximation of the final state within certain valid ranges of initial state and propagation time, the a priori estimated error is close to the exact error in sense of trend and magnitude, and the computational cost can be significantly saved by the weighted-order scheme without loss of accuracy.

Keywords: Orbit propagation; Differential Algebra; State transition polynomial; Taylor expansion

*Ph.D. Candidate, College of Aerospace Science and Engineering, National University of Defense Technology, Changsha 410073, China, sunzhj@nudt.edu.cn

†Assistant Professor, Department of Aerospace Science and Technology, Politecnico di Milano, 20156 Milano, Italy, pierluigi.dilizia@polimi.it

‡Professor, Department of Aerospace Science and Technology, Politecnico di Milano, 20156 Milano, Italy, franco.bernelli@polimi.it

§Professor, College of Aerospace Science and Engineering, National University of Defense Technology, Changsha 410073, China, luoyz@nudt.edu.cn

¶Engineer, Beijing Satellite Navigation Center, Beijing, China, linkunpeng@126.com

1 Introduction

As widely recognized, orbit propagation is a fundamental problem in astrodynamics. The initial orbital state under an orbital dynamics can be propagated [1–3] by numerical integration of the corresponding ordinary differential equation (ODE), or by an analytical or semi-analytical algorithm in some special cases. In many application scenarios involving orbit propagation, such as orbit determination, spacecraft navigation and control, space situational awareness, and robust trajectory optimization, the orbital states belonging to a domain around a reference trajectory are of interest. In such scenarios, propagating many points one by one may turn out to be computationally intensive and more efficient methods could be required. If the propagation time is fixed, several linear and nonlinear methods have been developed to provide a mapping from the initial state deviation to the final state [4–13]. However, if the propagation time also varies, meaning that the orbital state corresponding to displaced initial state and propagation time is needed, to authors' knowledge, the literature lacks an efficient and accurate method.

For the problem with fixed propagation time, the classic state transition matrix (STM) method [4,5] provides a linearized mapping of the initial state deviation to the final epoch. Several nonlinear methods have been developed in recent years to provide a higher-order version of this mapping. Thezse methods include differential algebra (DA) [6–9], the state transition tensor (STT) [10, 11], and the polynomial chaos expansion (PCE) [12, 13]. Moreover, a non-probabilistic set-theory convex modeling method was also developed by Wang et al. [14,15] to perform reliability analysis on uncertain-but-bounded parameters. Among these methods, DA supplies a powerful tool to automatically compute the high-order derivatives of a nonlinear function around a reference value. Thus, the high-order Taylor expansion of the function can be obtained [16], which brings up two advantages of the DA-based methods: 1) an arbitrary order can be selected and the plenty of terms of the high-order expansions is automatically handled in the DA framework; 2) the method would be self-adaptive to any regular nonlinear function, which may feature high-order derivatives that are hard to be derived manually. In the literature [6–9], the final state is approximated by a high-order Taylor polynomial with respect to the initial state, which is denoted as state transition polynomial (STP) in this work. The STP has been well used in many problems involving uncertain state propagation, such as to propagate uncertain sets of initial orbital states and compute collision probabilities by DA-based Monte Carlo simulation [6], to accurately estimate the moments of the final state uncertainty under different dynamics [7], and even to solve two-point boundary problems [8] and optimal control problems [9] in astrodynamics.

For the problem with variable propagation time, a linearized state and time transition matrix method is available in the literature [17–19]. Starting from the conventional STM, an additional term is added to include time perturbations and compute the associated time partial derivative [17], so that the corresponding STM terms for a time perturbation can be obtained. This turns out to be useful in linear guidance or covariance analysis with multiple event

triggers [18, 19]. Since orbital states usually show nonlinearity on time deviation, a novel high-order method is here introduced to propagate state variation throughout a relatively longer time duration. In the literature [20], an extended STP with time expansion based on the DA technique, denoted as STP-T in this work, was presented to compute the close encounter distance between the Earth and an asteroid. In this method, the STP-T is a high-order expansion of the final state with respect to initial state and propagation time, while the time deviation is still relatively small with respect to the total propagation time.

In this study, the STP-T method is further developed by introducing a weighted-order scheme, which allows STP-T to use different expansion orders on the different components with different nonlinearity, so that the validity range of time deviation can be enlarged. Then an a priori error estimation method for STP-T is presented, which is useful for selecting the order and determining the validity range of an STP-T. The paper is organized as follows. Firstly, a brief overview of the DA technique is provided in Sect. 2, and the method of STP with fixed time is introduced. Then, the DA-based STP-T method and the weighted-order scheme are presented in detail in Sect. 3. Subsequently, the a priori error estimation method is illustrated in Sect. 4. Finally, the accuracy and computational cost of the STP-T are analyzed in Sect. 5 under different typical orbital dynamics.

2 State Transition Polynomial with Fixed Time

2.1 Taylor Expansion of a Nonlinear Function

In the DA framework, by substituting the classical implementation of real algebra with the implementation of a new algebra of Taylor polynomials, any regular function f of n variables is expanded into its Taylor polynomial up to an arbitrary order k. The DA technique employed in this work was implemented in the free open-source software DACE [21].

Consider a generic n-dimensional, sufficiently regular, nonlinear function

$$\boldsymbol{y} = \boldsymbol{f}(\boldsymbol{x}) \tag{1}$$

and initialize $[\boldsymbol{x}]$ to be the DA counterpart of the independent variable $\boldsymbol{x}$ around its reference value $\bar{\boldsymbol{x}}$ by adding the perturbation $\delta\boldsymbol{x}$ to $\bar{\boldsymbol{x}}$, i.e.

$$[\boldsymbol{x}] = \bar{\boldsymbol{x}} + \delta\boldsymbol{x} \tag{2}$$

As can be seen from Eq. (2), $[\boldsymbol{x}]$ can already be interpreted as the Taylor expansion of $\boldsymbol{x}$ around the reference value $\bar{\boldsymbol{x}}$.

Substituting $[\boldsymbol{x}]$ into Eq. (1) and carrying out in the DA framework all the operations involved in the evaluation of $\boldsymbol{f}$ yield

$$\begin{aligned}[\boldsymbol{y}] &= \boldsymbol{f}([\boldsymbol{x}]) = \mathcal{T}_{\boldsymbol{y}}^{k}(\delta\boldsymbol{x}) \\ &= \sum_{p_1+\cdots+p_n\le k} \boldsymbol{c}_{p_1\ldots p_n} \cdot \delta x_1^{p_1} \cdots \delta x_n^{p_n}\end{aligned} \tag{3}$$

where $\mathcal{T}_{\boldsymbol{y}}^k$ is the kth order Taylor expansion of the dependent variable $\boldsymbol{y}$ with respect to $\delta\boldsymbol{x}$, $p_1, \ldots, p_n = 0, 1, 2, \ldots$ are the orders of components $\delta x_1, \ldots, \delta x_n$, and $\boldsymbol{c}_{p_1 \ldots p_n}$ are the Taylor coefficients of $\mathcal{T}_{\boldsymbol{y}}^k$:

$$\boldsymbol{c}_{p_1 \ldots p_n} = \frac{1}{p_1! \cdots p_n!} \cdot \frac{\partial^{p_1 + \cdots + p_n} \boldsymbol{f}}{\partial x_1^{p_1} \cdots \partial x_n^{p_n}} \tag{4}$$

When the orders of the components all equal 0, i.e. $p_1 = \cdots = p_n = 0$, the corresponding coefficient $\boldsymbol{c}_{p_1 \ldots p_n}$ is just the reference value $\bar{\boldsymbol{y}}$.

The evaluation of Eq. (3) at a selected value of $\delta\boldsymbol{x}$ supplies the kth order Taylor approximation of $\boldsymbol{y}$ corresponding to the displaced independent variable.

2.2 State Transition Polynomial of a Dynamical System

For a case where the state of a dynamical system is subject to a nonlinear ODE, the DA technique can also be used for automatic computation of the high-order Taylor expansion of the solution flow with respect to either the initial conditions or any parameter of the dynamics [8].

Consider the system state $\boldsymbol{x}$ subject to a nonlinear ODE

$$\begin{cases} \dfrac{d\boldsymbol{x}}{dt} = \boldsymbol{g}\left(\boldsymbol{x}, t\right) \\ \boldsymbol{x}\left(t_0\right) = \boldsymbol{x}_0 \end{cases} \tag{5}$$

where the initial state at time t_0 is $\boldsymbol{x}_0$.

By adopting a numerical integration scheme, such as the forward Euler's scheme, or the Runge-Kutta schemes, the final state $\boldsymbol{x}_f$ at time t_f can be computed. In the later numerical examples of this work, the 7/8 Dormand-Prince Runge-Kutta integration scheme is used. Hereafter, as an example for analysis, the forward Euler's scheme is considered,

$$\boldsymbol{x}_{k+1} = \boldsymbol{x}_k + \Delta t \cdot \boldsymbol{g}\left(\boldsymbol{x}_k, t_k\right) \tag{6}$$

where $k = 0, 1, 2, \ldots$

Initialize $[\boldsymbol{x}_0]$ to be the DA counterpart of the initial state $\boldsymbol{x}_0$ by adding the deviation $\delta\boldsymbol{x}_0$ to the reference initial state $\bar{\boldsymbol{x}}_0$.

$$[\boldsymbol{x}_0] = \bar{\boldsymbol{x}}_0 + \delta\boldsymbol{x}_0 \tag{7}$$

Substitute the initial state $[\boldsymbol{x}_0]$ into the first integration step, i.e.

$$[\boldsymbol{x}_1] = [\boldsymbol{x}_0] + \Delta t \cdot \boldsymbol{g}\left([\boldsymbol{x}_0], t_0\right) \tag{8}$$

If this step is carried out in the DA framework, the output, $[\boldsymbol{x}_1]$, is the Taylor expansion of the state $\boldsymbol{x}_1$ at time t_1 with respect to the initial state deviation $\delta\boldsymbol{x}_0$. The previous procedure can be iterated through the subsequent steps until the last integration step is reached. The result at the final step is the kth order

Taylor expansion of the solution flow $\boldsymbol{x}_f$ of the dynamic system in Eq. (5) at the final time t_f,

$$\begin{aligned}[\boldsymbol{x}_f] &= \mathcal{T}_{\boldsymbol{x}_f}^k \left(\delta \boldsymbol{x}_0\right) \\ &= \sum_{p_1+\cdots+p_n \leq k} \boldsymbol{c}_{p_1 \cdots p_n} \cdot \delta x_{0,1}^{p_1} \cdots \delta x_{0,n}^{p_n}\end{aligned} \tag{9}$$

where $\delta x_{0,i}\,(i = 1, 2, \ldots, n)$ are the ith components of the initial state deviation $\delta \boldsymbol{x}_0$. This high-order Taylor polynomial links the initial state deviation $\delta \boldsymbol{x}_0$ to the corresponding final state $\boldsymbol{x}_f$ and is referred to as state transition polynomial (STP) in this work.

3 State Transition Polynomial with Time Expansion

3.1 Numerical Integration along Normalized Time

In the above workflow, the final state is related to the initial conditions or any parameter of the dynamics while the propagation time is fixed. If the relation between the final state and the propagation time is also of interest, the dynamical system is properly modified to handle the propagation time as a general parameter in the DA framework [20].

Considering the initial value problem in Eq. (5), define a normalized time variable.

$$s = \frac{t - t_0}{t_f - t_0} \tag{10}$$

The differential of time t becomes

$$dt = (t_f - t_0)\, ds \tag{11}$$

By substituting Eq. (11) into the dynamics in Eq. (5), the nonlinear ODE becomes

$$\frac{d\boldsymbol{x}}{ds} = (t_f - t_0) \cdot \boldsymbol{g}\left(\boldsymbol{x}, t_0 + s\,(t_f - t_0)\right) \tag{12}$$

In this new ODE, the initial time t_0 and the final time t_f can be interpreted as general parameters of the dynamics.

Then, the numerical integration scheme, e.g. the forward Euler's scheme, becomes

$$\boldsymbol{x}_{k+1} = \boldsymbol{x}_k + \Delta s \cdot (t_f - t_0) \cdot \boldsymbol{g}\left(\boldsymbol{x}_k, t_0 + s_k\,(t_f - t_0)\right) \tag{13}$$

where $k = 0, 1, 2, \ldots$ The state is propagated from t_0 to t_f. Accordingly, the value range of the normalized time is $s \in [0, 1]$.

In addition to the initial state $\boldsymbol{x}_0$, the propagation time t_0 and t_f are also initialized as the corresponding DA counterparts by adding the perturbations

δt_0, δt_f to their reference values $\bar{t}_0$, $\bar{t}_f$, respectively, i.e.

$$\begin{cases} [\boldsymbol{x}_0] = \bar{\boldsymbol{x}}_0 + \delta \boldsymbol{x}_0 \\ [t_0] = \bar{t}_0 + \delta t_0 \\ [t_f] = \bar{t}_f + \delta t_f \end{cases} \tag{14}$$

The initial state $[\boldsymbol{x}_0]$, and the initial and final propagation times, $[t_0]$ and $[t_f]$, of Eq. (14) can now be inserted into the first integration step of Eq. (13), i.e.

$$[\boldsymbol{x}_1] = [\boldsymbol{x}_0] + \Delta s \cdot ([t_f] - [t_0]) \cdot \boldsymbol{g}\left([\boldsymbol{x}_0], [t_0] + s_0\left([t_f] - [t_0]\right)\right). \tag{15}$$

Carrying out this step in the DA framework and iterating this procedure to the last step, the output, $[\boldsymbol{x}_f]$, would be the kth order Taylor expansion of the solution flow with respect to both the initial state $\boldsymbol{x}_0$ and the initial and final propagation times t_0 and t_f,

$$\begin{aligned} [\boldsymbol{x}_f] &= \mathcal{T}^k_{\boldsymbol{x}_f}\left(\delta \boldsymbol{x}_0, \delta t_0, \delta t_f\right) \\ &= \sum_{p_1 + \cdots + p_{n+2} \le k} \boldsymbol{c}_{p_1 \cdots p_{n+2}} \cdot \delta x_{0,1}^{p_1} \cdots \delta x_{0,n}^{p_n} \cdot \delta t_0^{p_{n+1}} \delta t_f^{p_{n+2}} \end{aligned} \tag{16}$$

where $p_1, \ldots, p_{n+2}$ are the orders of the components $\delta x_{0,1}, \ldots, \delta x_{0,n}$ and $\delta t_0, \delta t_f$.

Thus, the kth order Taylor approximation of final state $\boldsymbol{x}_f$ can be obtained by evaluating $\mathcal{T}^k_{\boldsymbol{x}_f}$ of Eq. (16) at any selected initial state $\boldsymbol{x}_0$, initial time t_0 and final time t_f around their reference values. This Taylor polynomial is referred to as STP with time expansion (STP-T) in this work.

3.2 Weighted-Order Scheme for STP-T

From the form of the kth order STP-T in Eq. (16), it is found that all the components have the same potential maximum order, k. However in many cases, the final state shows different nonlinearity with respect to different components of initial state or propagation time. Consequently, for a given order k, the STP-T may show low accuracy on the components with higher nonlinearity, while the accuracy can be unnecessarily high for other components with lower nonlinearity. Therefore, in order to improve the accuracy on the components with higher nonlinearity and reduce the computational cost for the components with lower nonlinearity, a weighted-order scheme is combined with STP-T [22].

At first, the deviations of the initial state and propagation time are initialized as powers of the independent components in the DA framework, instead of the first power of them as in Section 3.1. Without loss of generality, the DA components related to the initial state are all initialized with the same order, whereas the components representing the time expansions are initialized with a different order, as in Eq. (17),

$$\begin{cases} \delta \boldsymbol{x}_0 = D^l_{\delta \boldsymbol{x}_0} \\ \delta t_0 = D^m_{\delta t_0} \\ \delta t_f = D^m_{\delta t_f} \end{cases}, \quad l, m = 1, 3, 5, \ldots \tag{17}$$

wherein the operator D represents the independent components in the DA framework, while l and m are the orders of the physical deviations on the DA components. In this way, the lth or mth power of a DA component represents the deviation of the corresponding independent physical variable. It should be noted that the values of l and m should be positive odd numbers, in order to guarantee the monotone increasing of the deviations of physical variables with respect to the corresponding DA components. Thus, the initial state and propagation time are initialized in the DA framework as follows.

$$\begin{cases} [\boldsymbol{x}_0] = \bar{\boldsymbol{x}}_0 + D^l_{\delta \boldsymbol{x}_0} \\ [t_0] = \bar{t}_0 + D^m_{\delta t_0} \\ [t_f] = \bar{t}_f + D^m_{\delta t_f} \end{cases}, \quad l, m = 1, 3, 5, \ldots \tag{18}$$

Then, similarly to Section 3.1, substituting Eq. (18) into the numerical integration scheme of Eq. (13) and performing the numerical integration in the DA framework yield the kth order Taylor expansion of the solution flow in the weighted-order scheme, i.e.

$$\begin{aligned} [\boldsymbol{x}_f] &= \mathcal{T}^k_{\boldsymbol{x}_f}\left(D^l_{\delta \boldsymbol{x}_0}, D^m_{\delta t_0}, D^m_{\delta t_f}\right) \\ &= \sum_{l\cdot p_1 + \cdots + m\cdot p_{n+2} \le k} \boldsymbol{c}_{l\cdot p_1 \ldots m\cdot p_{n+2}} \cdot D^{l\cdot p_1}_{\delta x_{0,1}} \cdots D^{l\cdot p_n}_{\delta x_{0,n}} D^{m\cdot p_{n+1}}_{\delta t_0} D^{m\cdot p_{n+2}}_{\delta t_f} \end{aligned} \tag{19}$$

where $p_1, \ldots, p_{n+2}$ are the orders of the deviations of the initial state and propagation time as in Eq. (16).

Thus, though the potential maximum order on the DA components in Eq. (19) is k, the maximum order on the initial state is $p_i = floor\left(\frac{k}{l}\right)$ for $i = 1, \ldots, n$, and the maximum order on the propagation time is $p_i = floor\left(\frac{k}{m}\right)$ for $i = n+1, n+2$. The function $floor\left(\cdot\right)$ means the maximum integer below a real number.

Overall, this weighted-order scheme supplies a useful method for the STP or STP-T to show different orders on different independent variables, where the order p_i on each variable is determined by initializing the deviations of the independent physical variables with different orders on the associated DA components.

4 Error Estimation of a State Transition Polynomial

When an STP-T is used to propagate the orbital state for a displaced initial state and propagation time, the order and the corresponding convergence radius of the STP-T need to be first determined according to the accuracy requirement. This means that the error of the high-order Taylor polynomial must be a priori estimated. In this section, a least-squares fit as in the literature [23] is performed to estimate the size of the coefficients of the $(k+1)$th order terms and the truncation error of the STP-T.

The approximation error between a $k+1$ times differentiable function f and its Taylor expansion P_f of order k, without loss of generality taken around the origin, is given by Taylor's theorem [24]:

$$|f(\delta x) - P_f(\delta x)| \leq C \cdot \delta x^{k+1} \tag{20}$$

where the constant $C > 0$ is the bound on the coefficient of the $(k+1)$th order term, i.e. $\left|\frac{f^{(k+1)}(x)}{(k+1)!}\right|, x \in [0, \delta x]$. This means that we can preliminarily estimate the error of a STP-T by approximately evaluating the size of the $(k+1)$th order terms.

As a direct consequence of Taylor's theorem, the coefficients of the Taylor polynomial expansion would decay exponentially independently of the function being expanded [23]. Hence in this work, an exponential fit of the size of all the known non-zero coefficients up to order k is performed to estimate the size of the $(k+1)$th order terms.

To be more precise, given a polynomial P of order k of the form

$$P(\boldsymbol{x}) = \sum_{\alpha} c_\alpha \boldsymbol{x}^\alpha \tag{21}$$

written using multi-index notation. In the case of multivariate polynomials $P(\boldsymbol{x}) = P(x_1, x_2, \ldots, x_n)$, the error with respect to component x_i is estimated. By evaluating the polynomial at certain values on the other components $x_1, \ldots, x_{i-1}, x_{i+1}, \ldots, x_n$, we have

$$P(x_i) = \sum_{j=0}^{k} c_{i,j} \cdot x_i^j \tag{22}$$

The size S_j of the term of order j is computed as the absolute value of the coefficient of exact order j

$$S_j = |c_{i,j}| \tag{23}$$

We denote by I the set of indices j for which S_j is non-zero. A least squares fit of the exponential function

$$f(j) = A \cdot \exp(B \cdot j) \tag{24}$$

is used to determine the coefficients A, B such that $f(j) = S_j, j \in I$ is approximated optimally in the least squares sense. Then the value of $f(k+1)$ is used to estimate the size S_{k+1} of the truncated order $k+1$ of P. The truncation error with respect to component x_i can be approximated by

$$e(x_i) = f(k+1) \cdot \left|x_i^{k+1}\right| \tag{25}$$

Moreover, for the weighted-order scheme of STP-T in Eq. (19), the polynomial in Eq. (22) can be reformulated as

$$P(D_{x_i}) = \sum_{j=0}^{j \leq k/m} c_{i,j} \cdot D_{x_i}^{m \cdot j} \tag{26}$$

where m is an odd positive number. For the orders that are not divisible by m, the corresponding coefficients are zero. Since only non-zero coefficients are counted in the least squares fit process, the size of the term of order $m \cdot ([k/m] + 1)$ is estimated, where $[k/m]$ means the integer part of k/m. That is to say, the truncation error of order $[k/m] + 1$ with respect to component x_i is then approximated by

$$e\left(x_i\right) = f\left(\left[\frac{k}{m}\right] + 1\right) \cdot \left| D_{x_i}^{m \cdot \left(\left[\frac{k}{m}\right]+1\right)} \right| \tag{27}$$

5 Numerical Simulations

5.1 Simulations under Different Dynamics

The presented STP-T is tested on orbit propagation problems involving typical orbital dynamical models, including the unperturbed Keplerian dynamics, the J_2 perturbed two-body dynamics, and the nonlinear relative dynamics with respect to a circular chief orbit. Moreover, for convenience, only the final propagation time is imposed to vary and the initial time is kept fixed.

In the following examples, the orbital states obtained by numerical integration are referred to as the exact solution. Additionally, the states around the reference final time obtained by STP-T are compared with the results of the Picard iteration method [16], which is a fixed-point iteration method for solving an ODE. More specifically, the Picard iteration method is implemented in the DA framework [25, 26] and supplies a high-order polynomial that relates the orbital state to the time around the reference epoch. The workflow of the DA-based implementation of the Picard iteration is reported in Appendix A.

5.1.1 Unperturbed Keplerian Dynamics

The unperturbed Keplerian dynamics is solved by numerically integrating the corresponding ODE model [1]:

$$\begin{cases} \dot{x} = v_x, \dot{y} = v_y, \dot{z} = v_z \\ \dot{v}_x = -\dfrac{\mu}{r^3} x \\ \dot{v}_y = -\dfrac{\mu}{r^3} y \\ \dot{v}_z = -\dfrac{\mu}{r^3} z \end{cases} \tag{28}$$

where $\boldsymbol{r} = [x, y, z]^{\mathrm{T}}$ and $\boldsymbol{v} = [v_x, v_y, v_z]^{\mathrm{T}}$ are the position and velocity vectors in the Earth-centered inertial (ECI) frame, and μ is the gravitational parameter of the primary.

To determine the initial reference Cartesian state of the spacecraft, the corresponding initial classical orbital elements are listed in Table 1. The reference orbit is a nearly circular orbit, and the inclination is close to 0 such that the

x-y plane is nearly the orbital plane. The reference orbital period is determined by the semi-major axis, i.e. $T = 5554$ s. The reference final propagation time is selected to be $\bar{t}_f = 10T$.

Table 1: Initial state under unperturbed Keplerian dynamics

a (km)	e	i (rad)	Ω (rad)	ω (rad)	θ (rad)
6778.137	0.001	0.001	0	0	0

Firstly, the final time t_f and the initial state $\boldsymbol{x}_0$ are initialized in the DA framework with the same order, as in Eq. (14). The maximum order is set to be $k = 4$. Thus the final STP-T is a 4th order Taylor approximation of the final state with respect to the displaced initial state and final time. By evaluating the STP-T at varying final time deviations, the orbital trajectory around the reference final time can be efficiently obtained. With a zero initial state deviation, the trajectory approximated by the STP-T is plotted and compared with the trajectories obtained by numerical integration in Fig. 1. Moreover, given the reference final orbital state, the trajectory around the reference final time can also be achieved by performing the Picard iterations, whose result is also reported in Fig. 1. From the figure, it can be seen that the STP-T trajectory approximates the exact trajectory, obtained with the numerical integration, for epochs close to the reference final time. The error increases for larger final time deviations δt_f. In addition, the trajectory described by the STP-T almost overlaps the trajectory obtained with the Picard iterations.

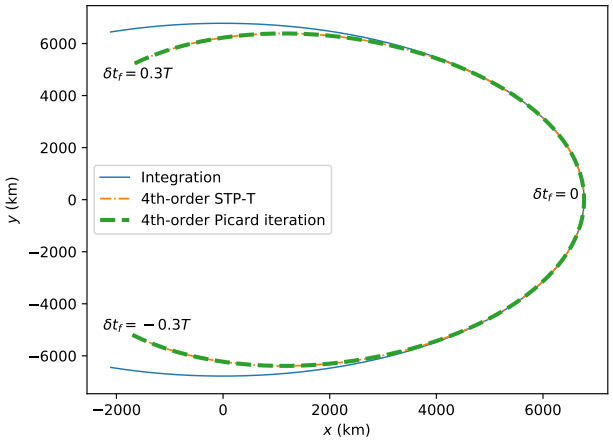

Figure 1: 4th-order approximate trajectory around the final time under unperturbed Keplerian dynamics

Then, to reduce the error of the polynomial approximation of the trajectory

over a larger domain of final time, the weighted-order STP-T is employed. By initializing the initial state and final time in the DA framework as in Eq. (18) with $k = 6, l = 3, m = 1$, the final STP-T supplies the 2nd-order approximation of the final state with respect to the initial state deviation, and the 6th-order approximation on final time deviation. Since the initial state deviation is set to zero, the resulting trajectory is a 6th-order approximation of the accurate orbit, which is shown in Fig. 2. We can see that the 6th-order trajectory approximates the exact trajectory significantly more accurately than its 4th-order counterpart.

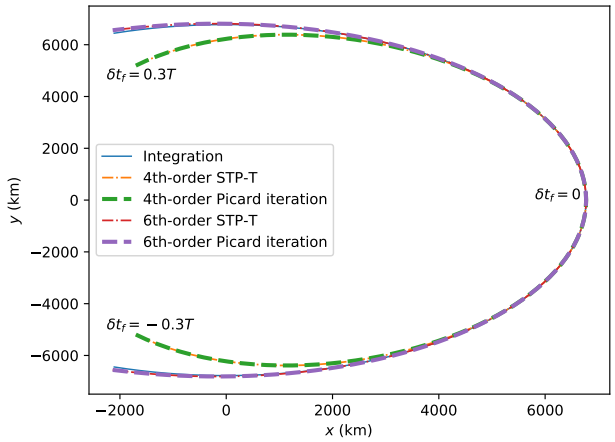

Figure 2: 6th-order approximate trajectory around the final time under unperturbed Keplerian dynamics

For the sake of completeness, the miss distances between the approximate trajectories and the numerically integrated one are shown in Fig. 3. Apparently, the error of the STP-T is close to the one of the Picard iterations at the same order. In addition, the error significantly decreases for higher-order expansions.

5.1.2 J2 Perturbed Two-Body Dynamics

The motion in a two-body dynamics considering J_2 perturbation is described by the following ODE [1].

$$\begin{cases} \dot{x} = v_x, \dot{y} = v_y, \dot{z} = v_z \\ \dot{v}_x = -\dfrac{\mu}{r^3}x - \dfrac{3\mu J_2 R_e^2}{2r^5}\left(1 - \dfrac{5z^2}{r^2}\right)x \\ \dot{v}_y = -\dfrac{\mu}{r^3}y - \dfrac{3\mu J_2 R_e^2}{2r^5}\left(1 - \dfrac{5z^2}{r^2}\right)y \\ \dot{v}_z = -\dfrac{\mu}{r^3}z - \dfrac{3\mu J_2 R_e^2}{2r^5}\left(3 - \dfrac{5z^2}{r^2}\right)z \end{cases} \tag{29}$$

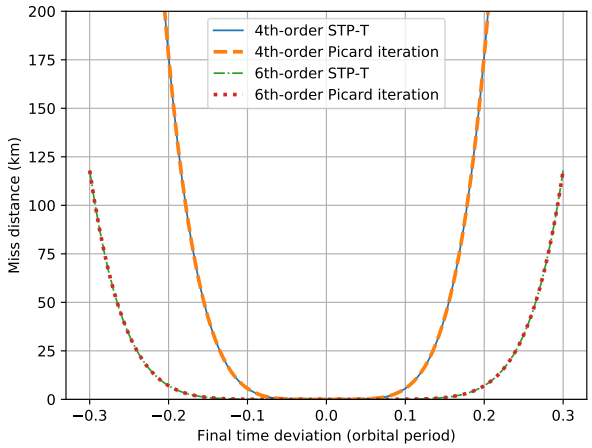

Figure 3: Miss distances of the approximate trajectories obtained with the STP-T and the Picard iterations around the reference final time under unperturbed Keplerian dynamics

where the 2nd-order zonal harmonic coefficient for the Earth is $J_2 = 1.08263 \times 10^{-3}$ and Earth's equatorial radius is $R_e = 6378.137$ km.

In this example, the initial classical orbital elements are listed in Table 2 and corresponds to an inclined elliptical orbit. The reference final propagation time is $\bar{t}_f = 10\,T$. The orders adopted to compute the STP-T to approximate the orbital state around the reference final time are $k = 6, 9, 12$.

In Fig. 4, the approximate trajectories around the reference final time with zero initial state deviation are compared with the exact trajectory from numerical integration. Similarly to Fig. 3, the corresponding miss distances are reported in Fig. 5. They illustrate the accuracy of the presented STP-T method under the J_2 perturbed two-body dynamics. When the final propagation time is close to the reference value, i.e. δt_f is close to zero, all the three approximate trajectories from STP-T are close to the numerically integrated one. As the final time deviation increases, i.e. towards the tails of the trajectories, the errors of the approximate trajectories increase. Moreover, apparently, the error of the STP-T decreases for increasing expansion orders: the approximate trajectory corresponding to the 12th-order expansion is the closest one to the exact trajectory in Fig. 4. Overall, the STP-T method has nearly the same error as the Picard iteration method at the same order.

Table 2: Initial state under J_2 perturbed two-body dynamics

a (km)	e	i (rad)	Ω (rad)	ω (rad)	θ (rad)
6778.137	0.2	$\frac{\pi}{4}$	0	0	0

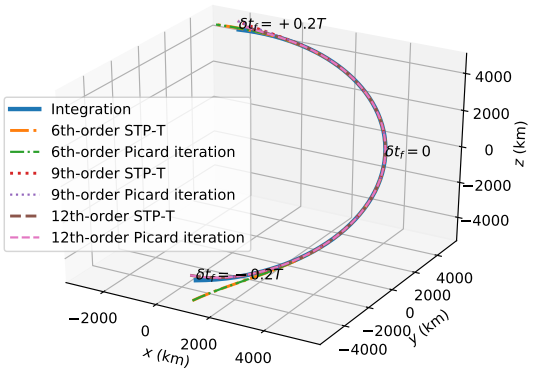

Figure 4: Approximate trajectories around the reference final time under J_2 perturbed two-body dynamics

5.1.3 Nonlinear Relative Motion with Circular Chief Orbit

In this subsection, the STP-T is tested under nonlinear relative dynamics. Two spacecraft are considered: one is termed *chief* and the other one is referred to as *deputy*. The motion of the deputy can be expressed in the local-vertical local-horizontal (LVLH) reference frame of the chief, and the *origin* is located at the center of mass of the chief; the x-axis is along the radial direction; the z-axis is along the angular momentum direction; and the y-axis completes the right-handed system. If the chief follows a circular orbit, the x-axis can also be called R-bar and y-axis can also be called V-bar, and the unperturbed relative motion is subject to the following ODE model [2]:

$$\begin{cases} \ddot{x} = 2n\dot{y} + n^2 x - \dfrac{\mu\left(a+x\right)}{\left[\left(a+x\right)^2 + y^2 + z^2\right]^{3/2}} + \dfrac{\mu}{a^2} \\ \ddot{y} = -2n\dot{x} + n^2 y - \dfrac{\mu y}{\left[\left(a+x\right)^2 + y^2 + z^2\right]^{3/2}} \\ \ddot{z} = -\dfrac{\mu z}{\left[\left(a+x\right)^2 + y^2 + z^2\right]^{3/2}} \end{cases} \tag{30}$$

where a represents the radius of chief orbit and n represents the orbital angular velocity of the chief.

In this example, the radius of the chief orbit is selected as $a = 6778.137$ km. An arbitrary initial relative state of the deputy is given in Table 3. The orders

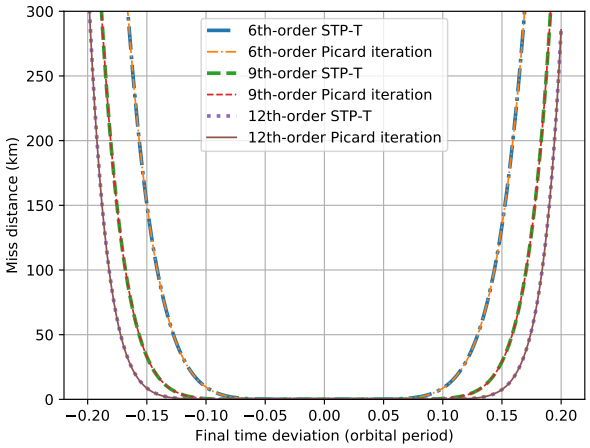

Figure 5: Miss distances of the approximate trajectories obtained with the STP-T and the Picard iterations around the reference final time under J_2 perturbed two-body dynamics.

adopted to compute the STP-T to approximate the orbital state around the reference final time are $k = 6, 9, 12$.

With a zero initial state deviation, the final trajectories after 10 orbital periods are plotted in Fig. 6 for $\delta t_f \in [-0.7\,T, +0.7\,T]$ to illustrate the accuracy of the STP-T under the nonlinear relative dynamics. The corresponding miss distances are shown in Fig. 7. The 6th-order approximate trajectory is close to the exact trajectory within a limited range of final time deviations: the error steeply increases when the time deviation is outside the STP-T validity range. As the order increases from 6 to 12, the validity range increases and the error is efficiently reduced. Similarly to the previous test cases, the STP-T method has nearly the same error as the Picard iteration method at the same order.

Table 3: Initial relative state of the deputy

x (m)	y (m)	z (m)	v_x (m/s)	v_y (m/s)	v_z (m/s)
0	0	0	5	5	0

Moreover, since the relative motion is a difference between the absolute motion of the two spacecraft, the relative dynamics shows lower nonlinearity than the absolute dynamics, such as in the previous unperturbed Keplerian dynamics and the J_2 perturbed two-body dynamics. Comparing the trajectories in Fig. 6 with the trajectories in Fig. 4, it can be seen that the validity range of the STP-T under nonlinear relative dynamics is larger than the range obtained under the J_2 perturbed two-body dynamics with the same order. Fig. 6 shows

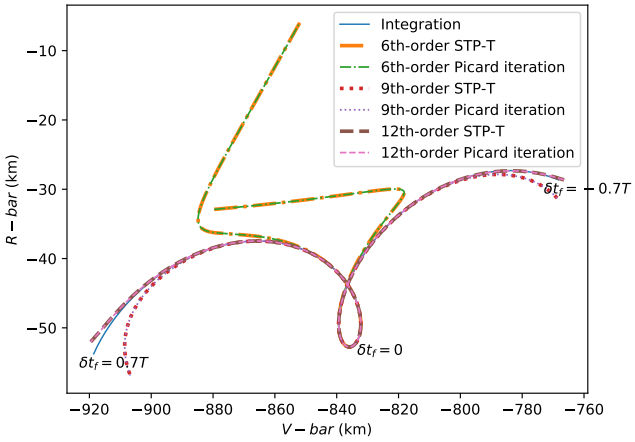

Figure 6: Approximate trajectories around the final time under nonlinear relative dynamics

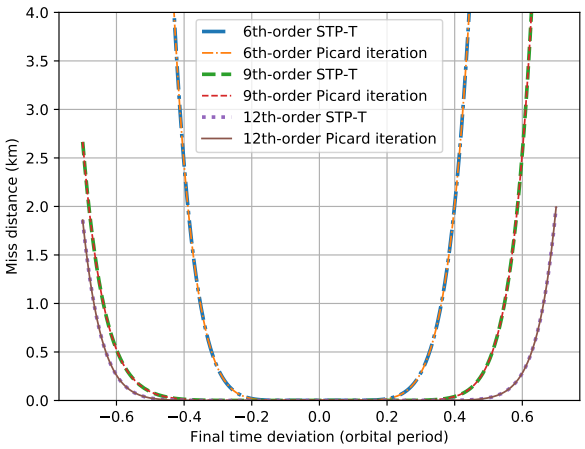

Figure 7: Miss distances of the approximate trajectories obtained with the STP-T and the Picard iterations around the reference final time under nonlinear relative dynamics

the trajectories around the reference final time within $\delta t_f \in [-0.7\,T, +0.7\,T]$, while Fig. 4 shows the trajectories only within $\delta t_f \in [-0.2\,T, +0.2\,T]$.

5.2 Sensitivity of Accuracy

Since the J_2 perturbed two-body dynamics shows higher nonlinearity than the unperturbed Keplerian dynamics and the nonlinear relative dynamics, the error of the STP-T is tested under the J_2 perturbed two-body dynamics in this section.

5.2.1 Error estimation

Considering the example in Section 5.1.2, the error of the STP-T for $k = 6, 9, 12$ with respect to final time deviations is analyzed with zero initial state deviation. First of all, the size of the coefficients of the higher order terms in STP-T are estimated by a least-squares fit as described in Section 4. The exact size of the coefficient of each order and the corresponding estimated one are compared in Fig. 8. The exact size for each order is reported as a bar in the figure. The 6-order estimation uses the exact sizes of the coefficients of orders from 0 to 6 to estimate the sizes of the coefficients of orders from 0 to 7. The exact size of the 7th order coefficient is considered as the reference. A similar approach is adopted for the 9th and the 12th-order estimations. As can be seen, the sizes of the 7th-order, 10th-order and 13th-order coefficients are approximated reasonably well by this method.

Then, the estimated size of the coefficients is used to approximately evaluate the higher order truncation error of the STP-T with respect to the final time deviation, according to Eq. (25). The exact error at a specific final time is instead obtained as the difference between the results of the STP-T method and the ones of the numerical integrations. Fig. 9 shows the estimated and exact errors on each component of the STP-T. It can be seen that the estimated error is close to the exact error in sense of trend and magnitude, though there are still some differences between them. Since the error estimation is performed a priori, it supplies a useful tool for selecting a proper order and determining the validity range of the STP-T according to the accuracy requirements for the specific application. Moreover, it can be seen that the error decreases with the order. In other words, given a fixed threshold on the error, higher-order STP-T has a larger validity range. It is also worth highlighting that the error of a STP-T increases exponentially with the final time deviation. For example, within the range $\delta t_f \in [-0.1\,T, +0.1\,T]$ in Fig. 9a, the error of the 12th-order STP-T on x_f is less than 100 m; when the final time deviation reaches about $\delta t_f = \pm 0.13\,T$, the error increases to about 1 km.

5.2.2 Error versus deviations on initial state and final time

In the followings, the accuracy of the STP-T is further assessed on both initial state deviation and final propagation time deviation. By initializing the initial

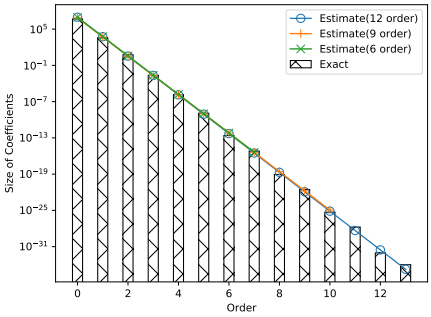

(a) Polynomial of $x_f\left(t_f\right)$

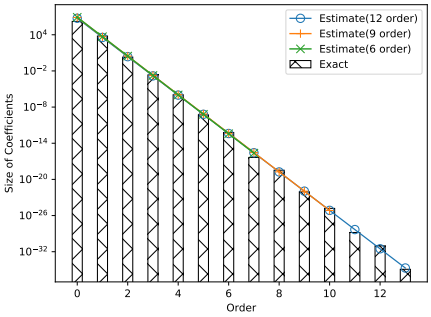

(b) Polynomial of $y_f\left(t_f\right)$

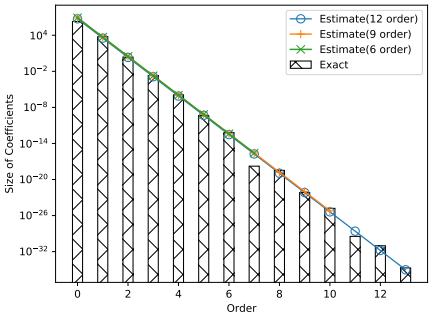

(c) Polynomial of $z_f\left(t_f\right)$

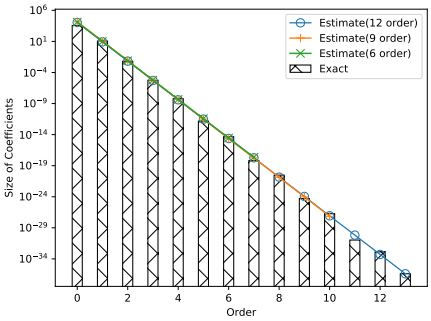

(d) Polynomial of $v_{x_f}\left(t_f\right)$

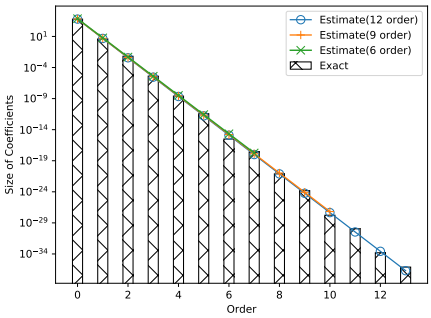

(e) Polynomial of $v_{y_f}\left(t_f\right)$

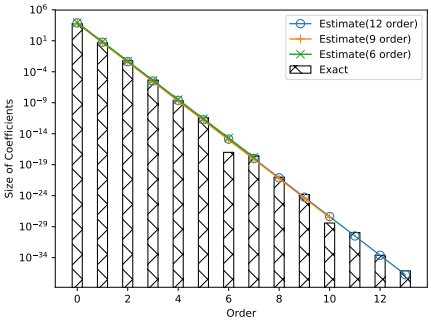

(f) Polynomial of $v_{z_f}\left(t_f\right)$

Figure 8: Estimation of the size of coefficients of the STP-T with respect to final time at each order under J_2 perturbed two-body dynamics

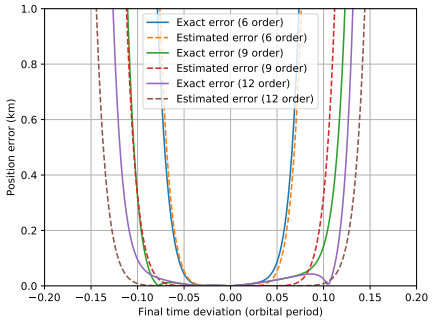

(a) Error on $x_f\left(t_f\right)$

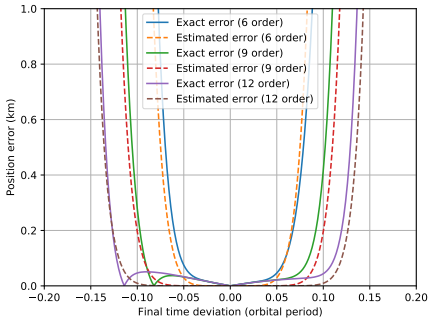

(b) Error on $y_f\left(t_f\right)$

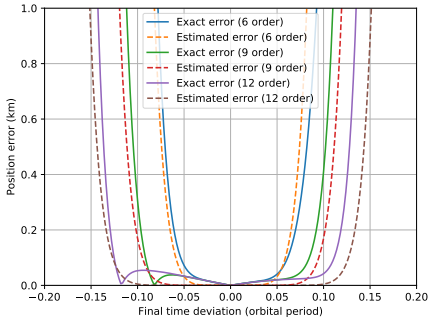

(c) Error on $z_f\left(t_f\right)$

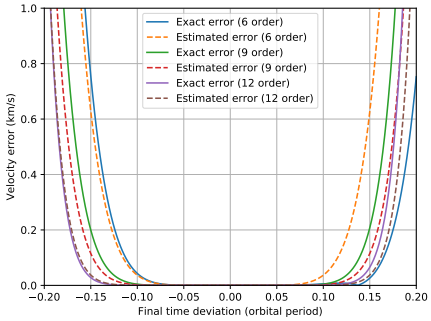

(d) Error on $v_{x_f}\left(t_f\right)$

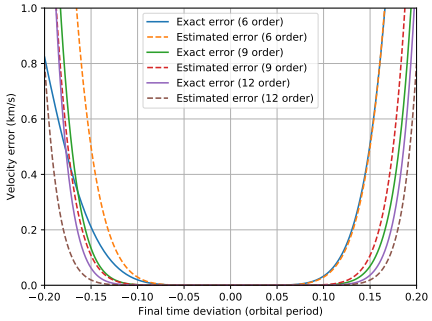

(e) Error on $v_{y_f}\left(t_f\right)$

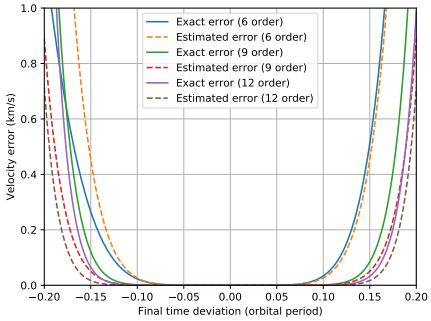

(f) Error on $v_{z_f}\left(t_f\right)$

Figure 9: Estimated and exact errors on each component of the STP-T around the final time under J_2 perturbed two-body dynamics

state and final time in the DA framework as in Eq. (18) with $k = 12, l = 3, m = 1$, the STP-T supplies the 4th-order approximation of the final state with respect to the initial state deviation, and the 12th-order approximation for the displaced final time. Without loss of generality, the initial reference state reported in Table 2 is adopted and the selected initial state deviations are listed in Table 4. Given the initial orbital state and propagation time, the miss distance between STP-T and numerical integration results is employed to assess the error of the STP-T. The variation of the miss distance with respect to the final propagation time is shown in Fig. 10.

Table 4: Deviations of the initial state under J_2 perturbed two-body dynamics

Case No.	Initial state deviation $\delta\boldsymbol{x}_0$ (m, m/s)
2BJ2-1	$[0, 0, 0, 0, 0, 0]^{\mathrm{T}}$
2BJ2-2	$[300, 0, 0, 3, 0, 0]^{\mathrm{T}}$
2BJ2-3	$[600, 0, 0, 6, 0, 0]^{\mathrm{T}}$
2BJ2-4	$[0, -300, 0, 0, -3, 0]^{\mathrm{T}}$
2BJ2-5	$[0, -600, 0, 0, -6, 0]^{\mathrm{T}}$

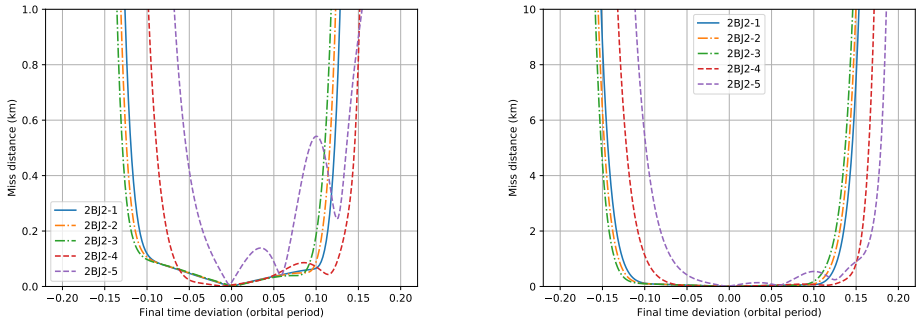

(a) Zoomed in

(b) Zoomed out

Figure 10: Miss distance of the STP-T corresponding to the initial state deviations in Table 4 under J_2 perturbed two-body dynamics

First of all, Fig. 10 seems to suggest that the initial state deviation may cause a bias on the validity range of the STP-T with respect to final time deviations, i.e. the validity range is no more centered at the reference final propagation time. For example, in Fig. 10a, with a threshold of 1 km on the miss distance, the validity range of the STP-T in Case 2BJ2-5 is about $\delta t_f \in [-0.07\,T, 0.15\,T]$. It is worth highlighting that in Cases 2BJ2-2 and 2BJ2-3 (or similarly in Cases 2BJ2-4 and 2BJ2-5) the initial state deviation in the latter case is larger and along the same direction with respect to the former (see

Table 4). From Fig. 10b, the larger deviation tends to exacerbate the bias of the validity range. In addition, in Cases 2BJ2-3 and 2BJ2-5, the initial state deviations are in different directions with equal magnitude. In this case, the biases tend to act in different directions on the final time deviation, and the bias in Case 2BJ2-5 is apparently larger. Furthermore, as the final time deviation increases, the miss distance increases faster for larger initial state deviations. For example in Fig. 10a, with a threshold of 1 km on the miss distance, the validity range in Case 2BJ2-5 is about $\delta t_f \in [-0.07\,T, 0.15\,T]$, which is smaller than the validity range in Case 2BJ2-4, approximately $\delta t_f \in [-0.10T, 0.15T]$.

5.2.3 Error versus propagation time

In the followings, the accuracy of the STP-T is assessed for different reference propagation times. With a reference propagation time of $\bar{t}_f = 5T, 10T, 15T$ respectively, the error profiles of the 12th-order STP-Ts for different final time deviations are shown in Fig. 11.

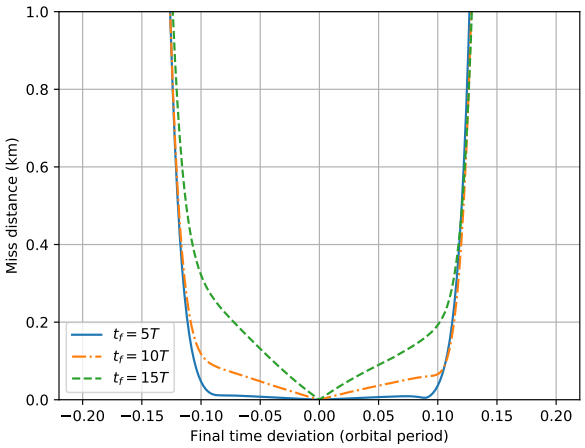

Figure 11: Miss distance of the approximate trajectories obtained with the STP-T corresponding to different reference propagation times under J_2 perturbed two-body dynamics

It can be seen that the STP-T tends to show larger errors for longer reference propagation times. Since there is no initial state deviation in this example, the error of the approximate trajectories obtained with all STP-Ts is zero at the reference final propagation time. As the final time deviation increases, the miss distance increases faster for STP-Ts with longer reference propagation times.

5.3 Sensitivity of Computational Cost

One possible application of the presented STP-T method is orbit propagation for replanning space missions online. If the high-order STP-T has been computed offline when designing the reference mission, the orbital state corresponding to the displaced actual initial state and propagation time can be acquired online by evaluating the Taylor polynomial, which is certainly much more efficient than the conventional numerical integration method.

When computing the high-order STP-T in the DA framework as in Eqs. (15), (16) and (19), the operation on the intermediate state $[\boldsymbol{x}_k]$ involves all the terms of the Taylor polynomial up to order k. For a kth order Taylor expansion with n independent variables, the number of terms is $(k+n)!/(k! \cdot n!)$, which increases with the order and the number of independent variables exponentially. Hence the integration of differential equations in the DA framework with a high order may also lead to a huge increase of the computational cost. The sensitivity of the computational cost to the order is investigated in this section.

According to the weighted-order scheme for STP-T in Section 3.2, the STP-T is actually a kth order Taylor polynomial, with order $floor\,(k/l)$ on the initial state deviation and $floor\,(k/m)$ on the propagation time deviation, where $l, m = 1, 3, 5, \ldots$. Usually, the final state shows higher nonlinearity in final time deviations than in initial state deviations. Thus, the parameter m is selected to be $m = 1$ in all the examples of this work, and the parameters k, l are selected according to the accuracy requirement and computational cost.

Figs. 12–14 show the times to compute the STP-Ts in Section 5.1 under the three typical dynamics, where k varies from 6 to 12, and l equals 1, 3, 5 respectively. All the computations are performed on a laptop with an Intel Core i7-6700HQ 2.60GHz CPU. As expected, the computation time increases exponentially with the order k. When $l = 1$, namely the STP-T has the same order for all components, the computation time would more than double as the order k increases by 1, which behaves similarly in all the three figures. Especially when $k \geq 10$, the computation time would increase to thousands of seconds, which are not computed and displayed in the figures.

If the weighted-order scheme is used, i.e. $l = 3, 5$, the computation time is significantly reduced, indicating that the purpose of presenting the weighted-order scheme is well reached. In addition, it is worth highlighting that the growth rate of the computation time with the order k decreases if the weighted-order scheme is adopted. When $l = 3, 5$, the computation time would less than double as the order k increases by 1. Moreover, the computation time of $l = 5$ is slightly smaller than the time of $l = 3$.

By comparing the computation time under the different dynamics in Figs. 12–14, it is found that the computation under the J_2-perturbed two-body dynamics is the most expensive one: it requires about twice the time needed for the computation under unperturbed Keplerian dynamics. On the other hand, the computation of the STP-T under nonlinear relative dynamics turns out to be the cheapest in terms of computation time.

Finally, the computation times of the STP-T and Picard iteration methods

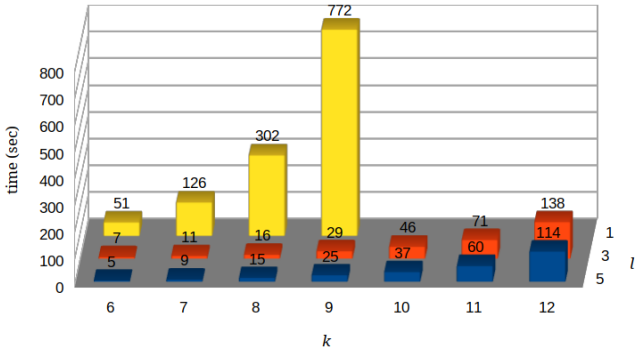

Figure 12: Computation time of the STP-T with different orders under unperturbed Keplerian dynamics

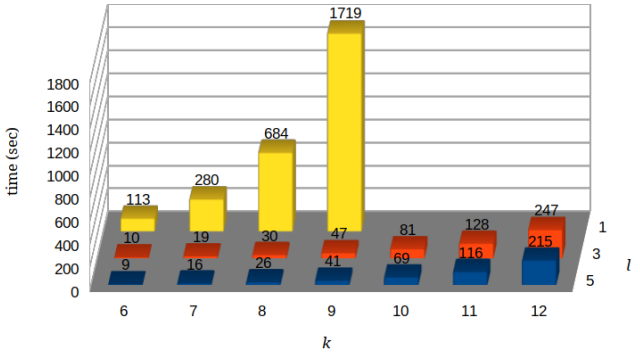

Figure 13: Computation time of the STP-T with different orders under J_2 perturbed two-body dynamics

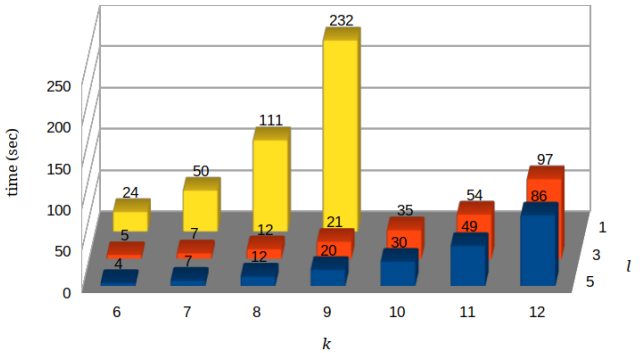

Figure 14: Computation time of the STP-T with different orders under nonlinear relative dynamics

with different orders under the J_2-perturbed two-body dynamics are shown in Fig. 15. When the orders of all independent components have the same weights, namely $l = 1$, the computation time of the STP-T is apparently larger than that of the Picard iteration method. When the weighted-order scheme is applied, namely $l = 3, 5$, there is no apparent difference on the computation time of the two methods. Actually, since only several times of iteration is needed, most computation time of Picard iteration is spent on the numerical integration from initial time $\bar{t}_0$ to final time $\bar{t}_f$. Then, the computation cost of numerical integration in Picard iteration is much less than STP-T, because there are 6 independent components (orbital state) in Picard iteration while there is one more independent component (final time) in STP-T. If the weighted-order scheme is applied in the numerical integration process, the total number of terms can be significantly reduced, making the computation faster and reducing the speed gap between the two methods.

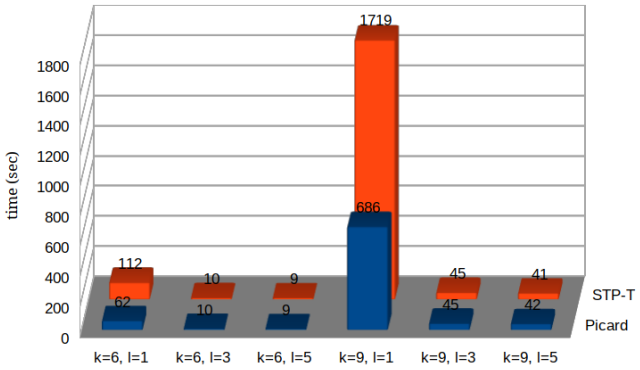

Figure 15: Computation time of the STP-T and Picard iteration methods with different orders under the J_2-perturbed two-body dynamics

6 Conclusions

A high-order state transition polynomial with time expansion (STP-T) method has been developed to analytically propagate an initial orbital state to a variable final time based on the use of the differential algebra (DA) technique. The STP-T is a high-order Taylor expansion of the final state with respect to both the initial state and the propagation time. Thus, the final state corresponding to any propagation time and initial state around their reference values can be directly computed by evaluating the STP-T, which is much more efficient than integrating each point of interest numerically. A weighted-order scheme is combined with STP-T, which allows higher expansion orders to be selected on components with higher nonlinearity, such that the computational cost can be significantly reduced without loss of accuracy. Furthermore, the error of an STP-T is a priori estimated by a least-squares fit of the size of terms of higher

orders, which supplies a useful tool for selecting a proper order and determining the validity range of the STP-T according to the accuracy requirement of the specific application.

Inherited from the features of the DA technique, the high-order derivatives of the differential equations are handled automatically in the method, hence it is self-adaptive to various dynamics and the order of the STP-T can be arbitrarily selected according to the accuracy requirement. The performance of the STP-T method has been tested under three typical orbital dynamics: the unperturbed Keplerian dynamics, the J_2 perturbed two-body dynamics, and the nonlinear relative dynamics. In the test cases, the presented STP-T method has the same error as the classic Picard iteration method at the same order. The sensitivity of the accuracy of the STP-T to deviations on initial state and propagation time has been investigated. The results indicate that the STP-T supplies a good approximation of the final state within the validity ranges of initial state and propagation time, the a priori estimated error is close to the exact error, and the error increases exponentially with the deviations. The analysis on the sensitivity of the computational cost demonstrated the effectiveness of the weighted-order scheme for the computation of the STP-T. Nevertheless, the Picard iteration method tends to be more efficient than the STP-T method in terms of computational time when the weighted-order scheme is not adopted.

Acknowledgements

This work was supported by the National Natural Science Foundation of China (Grant No. 11572345). Declarations of interest: none

Appendix A Workflow of the Picard Iteration Method with Differential Algebra

Considering the initial value problem in Eq. (5), the Picard-Lindelöf theorem shows that the Picard iteration

$$\begin{cases} \boldsymbol{\varphi}_0 := \boldsymbol{x}_0 \\ \boldsymbol{\varphi}_{j+1}(t) := \boldsymbol{x}_0 + \int_{t_0}^{t} \boldsymbol{g}\left(\boldsymbol{\varphi}_j, s\right) ds \end{cases} \tag{31}$$

converges to the solution flow $\boldsymbol{\varphi}(t)$ of the problem.

In the DA framework, an antiderivation operator ∂_i^{-1} is provided [16], which automatically computes the integration of a polynomial $[f(\boldsymbol{x})] = \mathcal{T}_f^k(\delta\boldsymbol{x})$ with respect to its ith component δx_i, i.e.

$$\partial_i^{-1}[f(\boldsymbol{x})] = \int_0^{\delta x_i} \mathcal{T}_f^k(\boldsymbol{s})\, ds_i \tag{32}$$

Thus, the workflow of Picard iteration method in the DA framework is formulated as follows.

- Initialize the time deviation as an independent DA component:

$$[t] = t_0 + \delta t \tag{33}$$

- Define the Picard operator $\Pi(\cdot)$ as

$$\Pi(\cdot) := \boldsymbol{x}_0 + \partial_t^{-1} \boldsymbol{g}(\cdot, [t]) \tag{34}$$

- Select the initial polynomial as the constant reference state

$$[\boldsymbol{\varphi}_0(t)] = \boldsymbol{x}_0 \tag{35}$$

- Iteratively compute the polynomial

$$\left[\boldsymbol{\varphi}_{j+1}(t)\right] = \Pi\left(\left[\boldsymbol{\varphi}_j\right]\right) \tag{36}$$

- After k steps, a polynomial $[\boldsymbol{\varphi}_k]$ invariant up to order k is obtained, i.e.

$$[\boldsymbol{\varphi}_k] =_k \left[\boldsymbol{\varphi}_{k+1}\right] = \Pi([\boldsymbol{\varphi}_k]) \tag{37}$$

  where $=_k$ means that the terms are equal up to order k.

According to the fixed-point theorem on DA [16], the Picard operator $\Pi(\cdot)$ is contracting on DA, then the fixed point of order k is exactly reached after k iterations as in Eq. (37). That is to say, the resulting polynomial $[\boldsymbol{\varphi}_k]$ supplies kth-order approximation of the orbital state $\boldsymbol{x}$ with respect to time deviation δt. Moreover, it is worth highlighting that, similarly to the STP-T method presented in this paper, the Picard iteration method can be extended to supply also the arbitrary order expansion of the orbital state with respect to the initial state.

References

[1] Pini Gurfil and P. Kenneth Seidelmann. *Celestial Mechanics and Astrodynamics: Theory and Practice*, volume 436 of *Astrophysics and Space Science Library*. Springer Berlin Heidelberg, Berlin, Heidelberg, 2016.

[2] Kyle T. Alfriend, editor. *Spacecraft Formation Flying: Dynamics, Control, and Navigation*. Elsevier astrodynamics series. Butterworth-Heinemann/Elsevier, Oxford, 2010.

[3] Mauro Pontani, Riccardo Di Roberto, and Filippo Graziani. Lunar orbit dynamics and maneuvers for Lunisat missions. *Acta Astronautica*, 149:111–122, 2018.

[4] Sangjin Lee, Hao Lyu, and Inseok Hwang. Analytical Uncertainty Propagation for Satellite Relative Motion Along Elliptic Orbits. *Journal of Guidance, Control, and Dynamics*, 39(7):1593–1601, 2016.

[5] Ohad Ben-Yaacov, Anatoly Ivantsov, and Pini Gurfil. Covariance analysis of differential drag-based satellite cluster flight. *Acta Astronautica*, 123:387–396, 2016.

[6] Alessandro Morselli, Roberto Armellin, Pierluigi Di Lizia, and Franco Bernelli Zazzera. A high order method for orbital conjunctions analysis: Monte Carlo collision probability computation. *Advances in Space Research*, 55(1):311–333, 2015.

[7] M. Valli, R. Armellin, P. Di Lizia, and M. R. Lavagna. Nonlinear mapping of uncertainties in celestial mechanics. *Journal of Guidance, Control, and Dynamics*, 36(1):48–63, 2013.

[8] P. Di Lizia, R. Armellin, and M. Lavagna. Application of high order expansions of two-point boundary value problems to astrodynamics. *Celestial Mechanics and Dynamical Astronomy*, 102(4):355–375, 2008.

[9] P. Di Lizia, R. Armellin, F. Bernelli-Zazzera, and M. Berz. High order optimal control of space trajectories with uncertain boundary conditions. *Acta Astronautica*, 93:217–229, 2014.

[10] K. Fujimoto, D. J. Scheeres, and K. T. Alfriend. Analytical nonlinear propagation of uncertainty in the two-body problem. *Journal of Guidance, Control, and Dynamics*, 35(2):497–509, 2012.

[11] Inkwan Park and Daniel J. Scheeres. Hybrid method for uncertainty propagation of orbital motion. *Journal of Guidance, Control, and Dynamics*, 41(1):240–254, 2018.

[12] Dirk M. Luchtenburg, Steven L. Brunton, and Clarence W. Rowley. Long-time uncertainty propagation using generalized polynomial chaos and flow map composition. *Journal of Computational Physics*, 274:783–802, 2014.

[13] Brandon A. Jones and Alireza Doostan. Satellite collision probability estimation using polynomial chaos expansions. *Advances in Space Research*, 52(11):1860–1875, 2013.

[14] Lei Wang, Xiaojun Wang, and Yong Xia. Hybrid reliability analysis of structures with multi-source uncertainties. *Acta Mechanica*, 225(2):413–430, 2014.

[15] Lei Wang, Xiaojun Wang, Ruixing Wang, and Xiao Chen. Reliability-based design optimization under mixture of random, interval and convex uncertainties. *Archive of Applied Mechanics*, 86(7):1341–1367, 2016.

[16] Martin Berz. *Modern Map Methods in Particle Beam Physics*. Academic Press, London, 1999.

[17] Wayne Tempelman. Properties of conic state transition matrices and associated time partials. *Journal of Guidance, Control, and Dynamics*, 7(2):135–140, 1984.

[18] Wayne Tempelman. Linear guidance laws for space missions. *Journal of Guidance, Control, and Dynamics*, 9(4):495–502, 1986.

[19] Renato Zanetti, David C. Woffinden, and Adam Sievers. Multiple Event Triggers in Linear Covariance Analysis for Spacecraft Rendezvous. *Journal of Guidance, Control, and Dynamics*, 35(2):353–366, 2012.

[20] R. Armellin, P. Di Lizia, F. Bernelli-Zazzera, and M. Berz. Asteroid close encounters characterization using differential algebra: the case of Apophis. *Celestial Mechanics and Dynamical Astronomy*, 107(4):451–470, 2010.

[21] Mauro Massari, Pierluigi Di Lizia, Francesco Cavenago, and Alexander Wittig. Differential algebra software library with automatic code generation for space embedded applications. In *2018 AIAA Information Systems-AIAA Infotech @ Aerospace*, number AIAA 2018–0398, 2018.

[22] Alexander Wittig and Roberto Armellin. High order transfer maps for perturbed Keplerian motion. *Celestial Mechanics and Dynamical Astronomy*, 122(4):333–358, 2015.

[23] Alexander Wittig, Pierluigi Di Lizia, Roberto Armellin, Kyoko Makino, Franco Bernelli-Zazzera, and Martin Berz. Propagation of large uncertainty sets in orbital dynamics by automatic domain splitting. *Celestial Mechanics and Dynamical Astronomy*, 122(3):239–261, 2015.

[24] Walter Rudin. *Principles of Mathematical Analysis*. McGraw-Hill, Inc., New York, 1976.

[25] Jens Hoefkens, Martin Berz, and Kyoko Makino. Computing validated solutions of implicit differential equations. *Advances in Computational Mathematics*, 19:231–253, 2003.

[26] Johannes Grote. *High-Order Computer-Assisted Estimates of Topological Entropy*. PhD thesis, Michigan State University, 2009.